Test Design Methodology for Time-Domain Immunity Investigations Using Electric Near-Field Probes

Xinglong Wu, *Member*, *IEEE*, Flavia Grassi, *Senior Member*, *IEEE*, Giordano Spadacini, *Senior Member, IEEE*, Sergio A. Pignari, *Fellow, IEEE,* Umberto Paoletti, *Senior Member*, *IEEE*, Isao Hoda, *Member*, *IEEE*

***Abstract*—This work investigates the possibility to develop time-domain immunity tests using electric near-field probes, for flexible customization of broadband input waveforms injected into specific pins of PCBs. For this purpose, a test design methodology is proposed, which is based on circuit modelling of the injection mechanism on the one hand, and on pulse design and equalization on the other hand. Two circuit models are developed. The former employs measurement/simulation data along with port-reduction techniques to model noise injection through near-field probes by means of internal induced sources. Conversely, the latter model only includes passive components, and is derived starting from physical observation of the involved phenomena. Both models are compatible with circuit solvers and can be easily adapted for different traces under test. Since pulse-like noise is usually broadband, suitable stress waveforms are utilized to obtain different noise spectra. Also, in order to precisely control the shape of the waveform reaching the targeted pin, an equalization procedure is employed. These models and techniques can be easily applied to amplification systems originally designed for frequency-domain tests, thus providing a comprehensive solution for the design of broadband immunity tests in the time domain. The feasibility and accuracy of the proposed methodology are proved by full-wave simulations and measurements.**

***Index Terms*—Circuit model, Microstrip line, Near-field probes, Pulse, Radiated Immunity.**

I. Introduction

As the scale of integration increases, electronic systems are moving to faster digital speed, and lower supply voltages and higher density of components are required. Moreover, for several applications, e.g., in the automotive sector, electronic devices are assigned more and more safety critical tasks. In such complex systems, susceptibility design margins of integrated circuits (ICs) are getting smaller while the electromagnetic (EM) environment is becoming severer. This demands the development of test procedures allowing to directly diagnose possible EM susceptibility issues at PCB or IC level. To this end, near-field probes, which were originally introduced to measure radiated EM fields [1], [2], can be conveniently applied also as injection devices for immunity assessment. This idea has received increasing attention since the last decade [3]. In [4] and [5], near-field probes were used for the analysis of EM susceptibility in chips. In 2014, the standard IEC TS 62132-9 was published [6], which includes an immunity procedure at IC level carried out through near-field scanning. The feasibility of using both electric and magnetic near-field probes for immunity verification at PCB level was investigated in [7] and [8], [9], respectively. A comparison of performance of different electric near-field (E-field) probes for immunity investigations is provided in [10].

Although most of the works on the subject are based on frequency-domain analysis, it is of great interest to investigate their immunity performance also to broadband impulsive waveforms. Indeed, pulse-like noise interferes with ICs in broadband spectra at almost the same time and consequently may lead to a failure different from single-frequency tests. Indeed, the actual waveforms that cause malfunction on a PCB is very different from the injected noise at system level, e.g., electrostatic discharge (ESD). Furthermore, to induce the same level of noise at the IC input through a continuous-wave signal, stricter requirements are imposed to the involved power amplifiers, resulting in more expensive equipment. Transmission line pulse (TLP) test tries to cover a broadband frequency range, but it is not very flexible in terms of waveforms and, therefore, of frequency content. Hence, there is the need for alternative methods allowing to flexibly select the input waveform at PCB level, along with some sets of waveforms suitable to test the PCB with severity but also efficiency in terms of time and injected power.

As a matter of fact, only few examples of impulsive stress waveforms are currently defined in the standards [11] and used in specific immunity procedures, such as ESD, TLP, surge, and electrical fast transient (EFT). In [12] and [13], near-field probes were employed to experimentally investigate on-board ESD issues, and the feasibility of this technique for immunity verification in time-domain was proven. However, many other sources of interference, either unintentional [14] or intentional [15], nowadays exist, which involve different kinds of broadband noise signals.

In this respect, another important aspect to be considered is the inherent difficulty to assure that the noise waveform actually induced at the input pins of the device under test (DUT) exhibits desired characteristics in terms of pulse width, rise and fall times, and duration. Indeed, before reaching the input pins of the DUT, the generated waveform might be significantly distorted due to the frequency response introduced by the injection device and due to noise propagation on the PCB under test as well as along the overall measurement chain.

To mitigate this issue, accurate broadband models of injection setups involving near-field probes need to be developed. Several models in the literature are unsuited for such a specific purpose, since the involved near-field probes are used as field sensors, and the objective is to derive equivalent radiated emission sources from near-field measurement [14], [16], [17]. Conversely, if the probes are used for noise injection, probe-to-trace electric coupling can be either modeled through a coupling capacitance [18], [19], [20], or an induced source [5], [21] determined by local-field distribution and field-to-wire coupling [22]. However, these models are inherently influenced by the specific characteristics of both the near-field probe and the trace under test, and therefore developing a new probe model for every test setup is quite time consuming. Also, in addition to capacitive coupling, other phenomena are involved, such as radiation, probe-to-ground coupling, etc., which require accurate modelling.

In this work, the possibility to develop an effective procedure for broadband immunity tests through the use of E-field probes is investigated, which involves the modelling of probe-to-trace coupling as the key-ingredient. To this end, two circuit models of the exploited electric near-field probe are proposed. The former is a behavioral model, whose parameters are extracted from measurement or full-wave 3D simulation of the probe mounted onto a reference PCB. The latter model (circuit-based model, in the following) provides a circuit representation of the physical phenomena involved in noise injection through near-field probes. Moreover, it will be proven that the values of model parameters, although initially estimated for a reference PCB structure, can be easily adapted to allow for accurate prediction in PCBs with different geometrical/electrical characteristics without the need for additional measurement or full-wave simulation. Two types of stress waveforms with different spectral characteristics are introduced to exemplify the proposed procedure. Also, an equalization method is introduced to derive the required waveforms to be set on the generator. The feasibility of the proposed procedure, that is its effectiveness in assuring the injection of stress waveforms with well-defined characteristics at the input pin of the DUT, will be assessed by measurement carried out resorting to an *ad hoc* conceived test bench set up in a semi-anechoic chamber.

The manuscript is organized as follows. Suitable models of the electric near-field probe under analysis are introduced in Section II (behavioral model) and Section III (circuit-based model). Section IV shows how probe-model parameters, although derived for a specific PCB under test, can be easily adapted for noise prediction in PCBs with different characteristics. Section V introduces suitable stress waveforms to be used for the test, and explains how these waveforms can be effectively induced at the input pins of the IC under test. In Section VI, feasibility of the proposed technique was assessed by measurements. Conclusions are eventually drawn in Section VI.

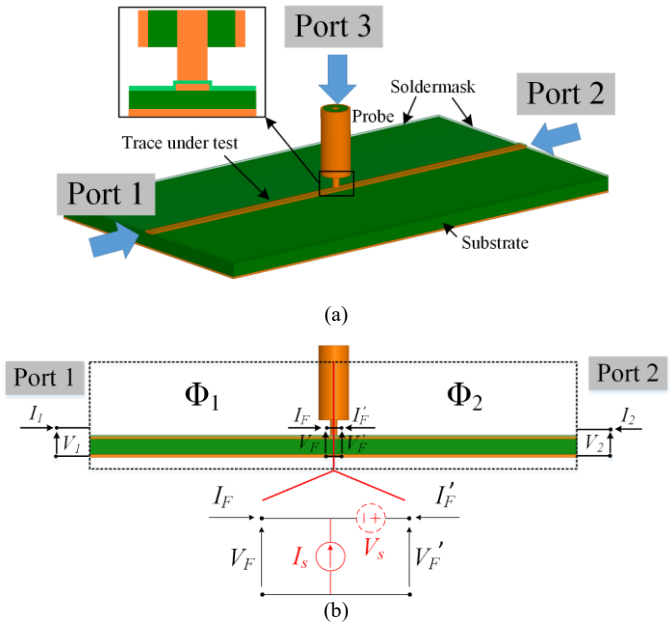

Fig. 1. Behavioral modelling of the near-field probe under analysis: (a) Reference injection setup (three-port network); and (b) Active two-port network (after port reduction), and circuit representation of near-field injection.

II. Behavioral Model

To derive a behavioral representation of the electric near-field probe under analysis, a reference structure involving a microstrip trace on top of a doubled-side PCB is considered, where the probe is placed at midpoint as shown in Fig. 1(a). The overall structure is characterized by measurement and/or full-wave simulation at the three output ports, and the obtained representation is converted into a two-port active network by the port-reduction technique originally introduced in [23] for the modelling of bulk current injection probes. The active and passive parts of the obtained representation are subsequently interpreted in terms of circuit elements, whose frequency response is directly extracted from measurement/simulation data.

A. Model derivation

With reference to the port numbering in Fig. 1(a), the *S*-parameter representation of the three-port structure under analysis writes:

$$\boldsymbol{S} = \begin{bmatrix} S_{11} & S_{12} & S_{13} \\ S_{12} & S_{11} & S_{13} \\ S_{13} & S_{13} & S_{33} \end{bmatrix} \tag{1}$$

where the equalities $S_{12} = S_{21}$ and $S_{11} = S_{22}$ hold due to reciprocity and symmetry of the setup, respectively. Moreover, the equality $S_{23} = S_{13}$ reflects not only the absence of directivity

of the probe, but also the inherent symmetry of its structure, unlike for instance in [23], where these two parameters were equal in magnitude but opposite in phase.

Starting from (1), an active two-port representation seen from the trace under test, Fig. 1(b), is obtained by assuming a non-ideal voltage source (with internal parameters: V_{RF}, and $R_0 = 50$ Ω) connected to the input port of the probe, and by eliminating the corresponding port. This yields:

$$\begin{bmatrix} b_1 \\ b_2 \end{bmatrix} = \begin{bmatrix} S_{11} & S_{12} \\ S_{12} & S_{11} \end{bmatrix} \cdot \begin{bmatrix} a_1 \\ a_2 \end{bmatrix} + \frac{S_{13} V_{RF}}{2\sqrt{R_0}} \begin{bmatrix} 1 \\ 1 \end{bmatrix}, \tag{2}$$

where a_1, a_2 and b_1, b_2 are the incident and reflected waves at port 1 and 2, respectively, and $R_0 = 50$ Ω denotes the reference impedance introduced to define the S-parameters. Converting (2) into chain-parameter notation leads to the expression:

$$\begin{bmatrix} V_2 \\ -I_2 \end{bmatrix} = \mathbf{\Phi} \cdot \begin{bmatrix} V_1 \\ I_1 \end{bmatrix} + \mathbf{F};\ \mathbf{F} = \begin{bmatrix} -S_{11} + S_{12} - 1 \\ \dfrac{-S_{11} + S_{12} + 1}{R_0} \end{bmatrix} \frac{S_{13} V_{RF}}{2S_{12}}, \tag{3}$$

where V_1, V_2 and I_1, I_2 are the voltages and currents at port 1 and 2, respectively, $\mathbf{\Phi}$ is a 2×2 matrix representative for the passive part of the model, and involving the S-parameters S_{11}, S_{12} only, whereas vector $\mathbf{F}$ represents the active part, that is the RF energy injected by the probe on the trace under test.

As suggested in Fig. 1(b), if the two trace sections by the sides of the probe are modeled as transmission lines with chain parameter matrices $\mathbf{\Phi}_1 = \mathbf{\Phi}_2$, (3) can be re-written as:

$$\begin{bmatrix} V_2 \\ -I_2 \end{bmatrix} = \mathbf{\Phi}_2 \cdot \mathbf{\Phi}_1 \cdot \begin{bmatrix} V_1 \\ I_1 \end{bmatrix} + \mathbf{\Phi}_2 \begin{bmatrix} V_S \\ I_S \end{bmatrix}, \tag{4}$$

where the voltage and current sources V_S and I_S are introduced to provide the mechanism of RF injection by near-field probes with a (general) circuit representation.

Theoretically, the effect of perturbation exerted by the presence of the probe on the transmission characteristics of the trace under test should be taken into account. However, previous investigations [9] carried out by measurement and simulation on injection setups involving electric-field probes proved that, as long as the trace under test is covered by the solder mask (non-contact test in [9]), the probe exerts a negligible effect on signal propagation on the trace under test (i.e., the test is not intrusive). Hence, this effect can be neglected. Moreover, (3) and (4) suggest the net prevalence of the current source I_S over the voltage source V_S in the active part of the model, as it will be investigated in the next sub-section by means of a suitable example.

B. Parameters of the behavioral model for the reference structure

To exemplify the procedure of identification of the parameters of the behavioral model, an electric near-field probe, realized by a semi-rigid cable RG405 11.75 mm long and terminated in a 1 mm tip (hereinafter referred to as "probe RG405") is considered. The definition of probe performance parameters for immunity tests and their experimental investigation for probe RG405 can be found in [9].

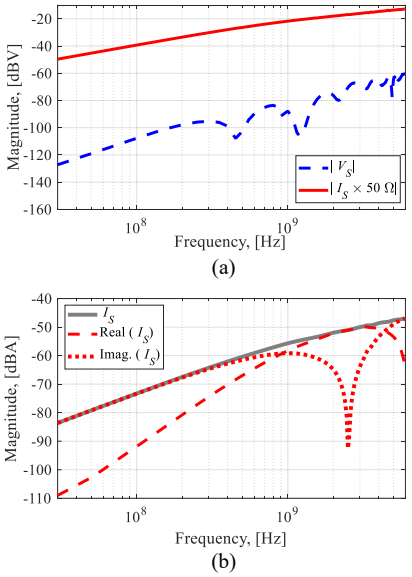

Fig. 2. Behavioral model parameters of the electric near-field probe RG405: (a) Comparison between the induced sources V_S and I_S. (b) Magnitude, real and imaginary parts of I_S.

The probe is placed at midpoint of a microstrip PCB land hereinafter considered as reference structure, and characterized by the following parameters: trace width $w = 0.511$ mm, trace length $L = 149$ mm, copper thickness $t = 35$ µm, substrate thickness $h = 80$ µm, substrate material FR4 ($\varepsilon_r = 4.7$, $tan\delta = 0.014$). An FR4 solder mask with thickness $t_{mask} = 30$ µm is covering the PCB traces.

For such a structure, numerical simulations by Ansys HFSS were carried out to obtain the entries of three-port S-parameter matrix in (1) as well as the S-parameters, and hence the chain-parameter matrices in (4), at the PCB trace terminals in the absence of the probe, so to extract (by post-processing of simulation data) the induced sources V_s and I_s.

The obtained frequency responses are plotted in Fig. 2(a), where the negligibility of the voltage source V_s with respect to the current source I_s (here multiplied by 50 Ω to be directly compared vs the voltage source) can be clearly appreciated in the whole frequency interval up to 6 GHz. Therefore, hereinafter a behavioral model comprising only the induced current source I_s will be considered, whose magnitude, real, and imaginary parts are plotted in Fig. 2(b). The figure shows that, as expected, capacitive coupling is the dominant effect at low frequency (i.e., nearly up 1 GHz). At high frequency, however, also other phenomena contribute to determining the frequency response of the I_S, which cannot be longer modeled through a capacitor only.

III. Circuit-Based Model

Starting from the behavioral model previously extracted, in this Section a circuit-based model of the injection setup in Fig. 1 is developed, based on circuit interpretation of the coupling paths involved in near-field injection.

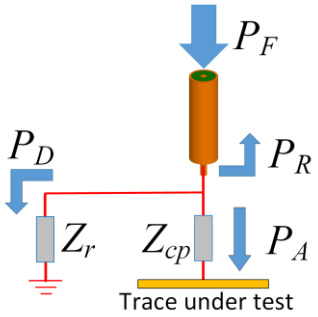

Fig. 3. Principle drawing outlining the coupling paths modeled by the proposed circuit-based model.

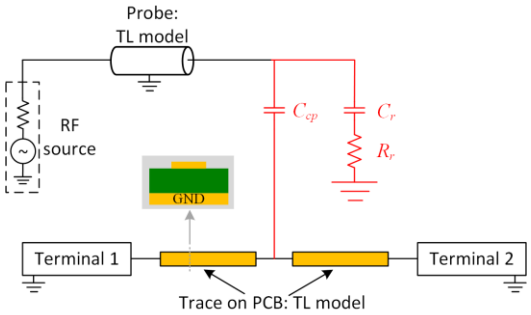

Fig. 4. Circuit-based model of the injection setup in Fig. 1, implemented in Keysight ADS.

A. *Basic principles*

With reference to the injection setup in Fig. 1, the forward power (P_F) at the input of the near-field probe can be written as

$$P_F - P_R = P_A + P_D \tag{5}$$

where P_R is the power reflected by the discontinuity introduced by the probe tip, P_A is the actual power injected into the trace under test (i.e., the absorbed power), and P_D denotes the dissipated power, e.g., the power dissipated due to radiation and possible coupling with the PCB ground and the probe shield. The corresponding principle diagram is shown in Fig. 3, where the lumped impedances Z_{cp}, Z_r are associated with P_A and P_D, respectively.

An optimization procedure will be presented in the next sub-section to fit the frequency responses of these impedances by lumped circuit elements. Conversely, distributed-parameter models based on transmission line theory, will be applied to model the probe and the trace under test.

B. *Optimization procedure and numerical results*

In order to fit the frequency responses of impedances Z_{cp} and Z_r by lumped circuit elements, an initial guess concerning their circuit representation along with reasonable initial estimates of the values of the involved circuit components is required.

As far as Z_{cp} is concerned, this is achieved by observing that, as long as coaxial E-field probes are considered, capacitive coupling between the probe and the trace under test is the dominant effect. Hence, Z_{cp} is initially modeled through a capacitor, whose (initial) value is estimated by resorting to electrostatic 3D simulation limited to the coupling area.

Conversely, an initial circuit representation of the impedance Z_r is obtained by considering the coaxial E-field probe under analysis in the absence of the PCB. Numerical simulations proved that the probe radiation properties can be equivalently represented by a complex impedance, Z_{r0}, connected with the probe tip. Particularly, evaluation of the reflection coefficient at the probe input (in free space) allows modelling Z_{r0} as the connection of a capacitor C_r in series with a resistor R_r, as shown in Fig. 4. The values obtained by free-space simulation are then used as initial values for the optimization, as the presence of the PCB is expected to significantly modify the near-field distribution, and hence the actual values of C_r and R_r. The goal of the optimization is set so that the current through Z_{cp} is equal to the complex value of the current source I_s obtained in Sec. II.

Based on the above considerations, an optimization procedure can be run. Without loss of generality, optimal values for Z_{cp}, C_r, R_r were automatically tuned by using the "optimization" functionality with gradient method available in Keysight ADS. To simplify the procedure, a probe length of 2 mm instead of the actual length was considered during the optimization. The real part of Z_{cp} proves to be close to zero, and therefore the final circuit-based circuit model of the injection setup is shown in Fig. 4. For the specific probe and PCB introduced in Sec. II. B, the procedure yields the values: C_{cp} = 0.3393 pF, C_r = 1.104 pF, R_r = 16.46 Ω.

IV. Tuning Model-Parameters to Different Test Setups

This Section will prove that the parameters of the behavioral and circuit-based probe models can be easily adapted and successfully used for prediction in setups involving PCB traces with characteristics different from those of the reference structure. To this end, a frequency-independent correction factor will be introduced, and different PCB samples will be exploited to prove model effectiveness in predicting the actual noise injected at the terminations of the trace under test.

A. *Correction Factor*

Starting from the observation that RF energy transfer to the trace under test is mainly due to capacitive coupling, the correction factor

$$\delta = \frac{C}{C_{ref}} \tag{6}$$

is introduced as the ratio between the probe-to-trace mutual capacitance in the actual test setup, C, and in the reference structure, C_{ref}. These capacitances are easily calculated by means of electrostatic simulation of the coupling area comprising the probe tip and the trace under test.

The correction factor in (6) can be used to tune both the parameters of the behavioral model and those of the circuit-based model to the characteristics of the actual PCB under test. For the behavioral model, the actual value of the induced current source, I_S^{new}, is obtained from the value extracted for the reference structure, I_S^{ref}, as

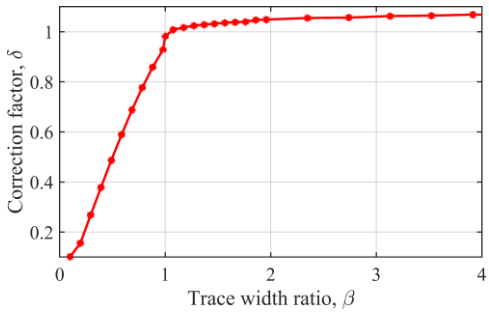

Fig. 5. Correction factor (δ) for the near-field probe RG405 as function of the trace-width ratio β.

$$I_S^{new} = \delta I_S^{ref} \ . \tag{7}$$

For the circuit-based models, updated values for the involved circuit elements are obtained in a similar fashion, by using the empirical relationships:

$$C_p^{new} = \delta C_p^{ref} \ , \ C_r^{new} = \delta C_r^{ref} \ , \ R_r^{new} = \delta R_r^{ref} \ , \tag{8}$$

To investigate the sensitivity of the correction factor in (6) to the actual size of the trace, a trace-width ratio β is introduced as:

$$\beta = \frac{w_{new}}{w_{ref}}, \tag{9}$$

where w_{new} and w_{ref} denote the widths of the actual and the reference traces, respectively. Without loss of generality, in the analysis, a reference width equal to the probe-tip diameter is selected, i.e., $w_{ref} = 0.511$ mm.

The obtained correction factor, δ, as function of β is plotted in Fig. 5, and exhibits a piece-wise linear behavior. Namely, the correction factor linearly increases with β as long as the width of the actual trace is smaller than the probe tip (i.e., as long as β <1). Conversely, for larger trace widths, the correction factor keeps an almost constant value, equal to nearly 1.07 for the specific near-field probe under analysis.

B. Validation of the proposed correction factor

To validate the effectiveness of the proposed correction factor, different PCB samples are considered, whose geometrical/electrical characteristics are collected in Tab. 1. The first and second samples involve traces with width smaller and larger than the reference one, respectively. Conversely, in the third example, also the substrate material and thickness are changed.

For validation, the probe was always placed at midpoint of the trace under test and in contact with the solder mask (material: FR4, nominal thickness: 30 µm) covering the trace. The transmission coefficient, S_{13}, predicted by full-wave simulation (Ansys HFSS) was compared versus the prediction obtained by the behavioral and circuit-based models with parameters adapted according to (7) and (8), respectively. For the three test cases in Tab. I, the exploited correction factors were: 0.6880, 1.0645, and 1.0645, respectively. The

TABLE I VALIDATION EXAMPLES.

Example	Reference	#1	#2	#3
Trace width	0.511 mm	0.3 mm	1.8 mm	1.8 mm
Substrate material	FR4 ($\varepsilon_r = 4.7$, $tan\delta = 0.014$)			Rogers RO4350B ($\varepsilon_r = 3.66$, $tan\delta = 0.004$)
Substrate thickness	80 µm			1524 µm

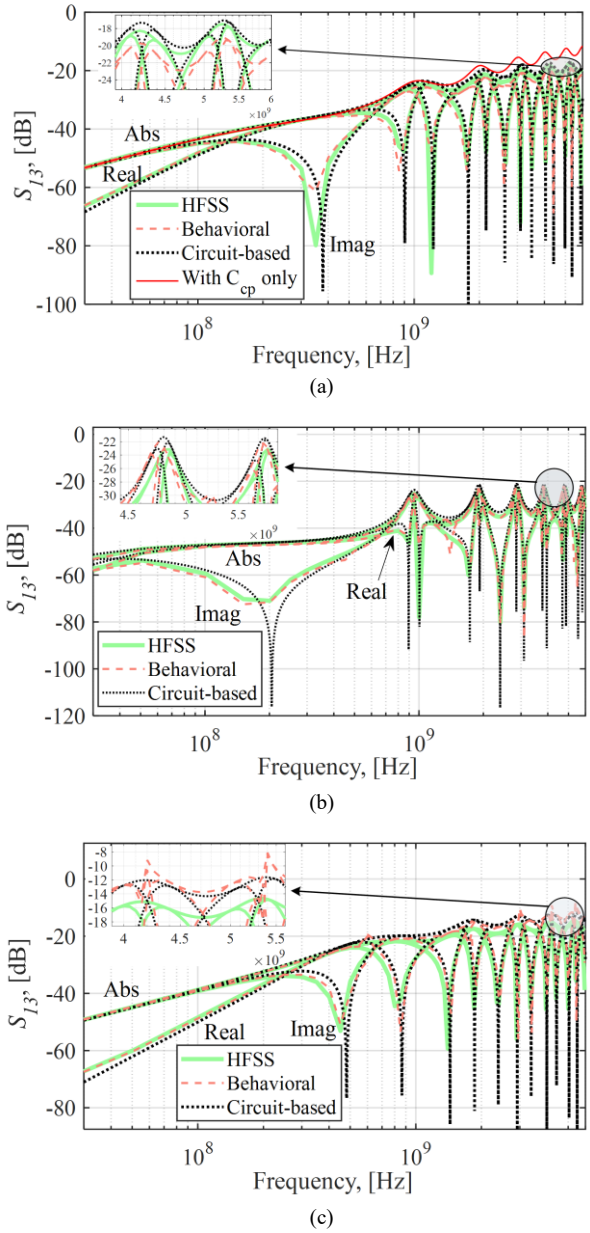

Fig. 6. Prediction of the probe-to-trace transmission coefficient obtained by full-wave simulation (HFSS), behavioral and circuit-based models for the three PCB samples in Table I: (a) #1 (b) #2, and (c) #3.

comparisons between full-wave simulations and model predictions plotted in Fig. 6 show excellent agreement except at the anti-resonances, where differences are observed in the imaginary part. However, at these frequencies, the imaginary part is negligible, and the observed differences negligibly impact on the injected time-domain waveforms, as it will be proven in the following sections. This confirms the

effectiveness of the introduced correction factor to tune model parameters in the frequency range of interest for the test, that is up to 6 GHz [6]. For the sake of comparison, the prediction obtained by only retaining capacitor C_{cp} in the circuit-based model is also plotted in Fig. 6(a), to stress out the important role played by the other circuit elements in assuring accurate prediction.

V. Design and Injection of Suitable Stress Waveforms

Exploiting wideband signals to assess the susceptibility of electronics components is nowadays receiving increasing attention from the EMC community, since the standard procedures for immunity verification, resorting to modulated sinusoidal signals only, can provide just partial information on the actual immunity characteristics of DUTs. In principle, depending on the specific sector, a set of suitable stress waveforms should be determined and customized by experimental characterization of the electromagnetic environment the DUT is expected to be immersed in during its operation.

However, since such a survey is beyond the objectives of this study, without loss of generality, feasibility of the proposed procedure of testing will be exemplified here by making use of narrow and broadband Gaussian-pulse waveforms as well as suitable combinations of them.

A. *Stress waveforms exploited for the test*

In the remainder of this work, two types of stress waveforms will be applied, to exemplify the basic principles of the test, and to prove the effectiveness of the proposed modelling approach to assure the injection of stress waveforms with specified characteristics at the input pins of the IC under test.

The two Gaussian-modulated pulses shown in Fig. 7 are firstly considered, characterized by the same center frequency, f_c and different fractional bandwidth, *FBW*. Use of these waveforms is intended to investigate possible DUT susceptibility to impulsive waveforms, whose energy is mainly concentrated in a frequency interval around a given center frequency. Then, an *ad hoc* stress waveform was introduced, whose main characteristic is to exhibit a flat frequency response over an assigned frequency interval, thus assuring simultaneous injection of several spectral components at the input pins of the IC under test. This is achieved by combining (i.e., summing up) multiple single Gaussian-modulated pulses in the time domain, and will be hereinafter referred to as "Gaussian-combination" in the following. An example is shown in Fig. 8, where 38 Gaussian-modulated pulses were summed up in the time domain in order to obtain a resultant waveform, Fig. 8(c), with a flat spectrum, Fig. 8(d) in the interval from 30 MHz up to 400 MHz. The characteristics of the specific waveforms exploited in this work for experimental validation of the procedure are collected in Table II and Table III.

B. *Equalization procedure*

To generate the waveforms foreseen by the proposed test procedure, an Arbitrary Waveform Generator (AWG) with a suitable bandwidth can be conveniently employed. However, since the generated waveforms are expected to be non-negligibly distorted by the overall transfer function due to the measurement chain, an equalization procedure is required. Indeed, given one of the previous waveforms as the output

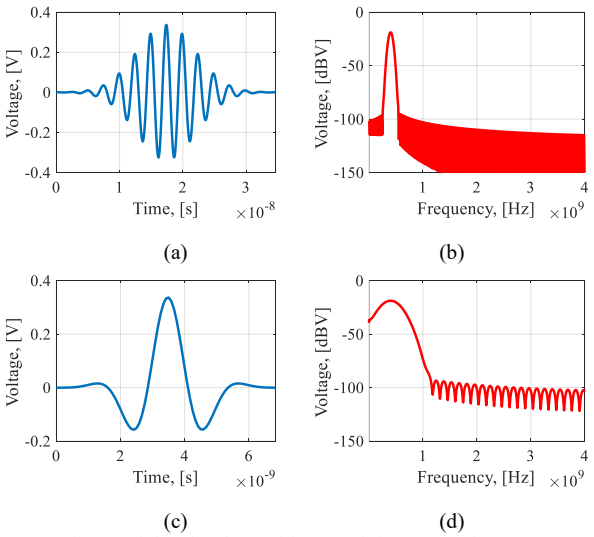

Fig. 7. Gaussian-modulated pulses with central frequency f_c = 400 MHz and fractional bandwidth (a), (b) *FBW* = 0.2, and (c), (d) *FBW* = 1: waveform (left panels) and corresponding spectrum (right panels).

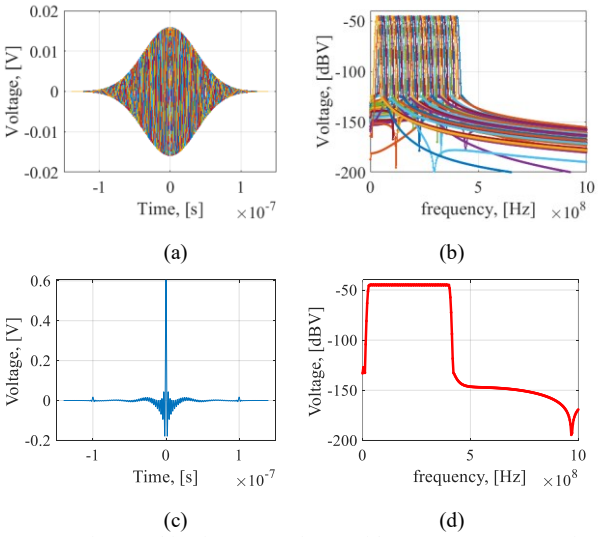

Fig. 8. "Gaussian-combination" waveform with constant spectrum in the interval 30 MHz~400 MHz. Original Gaussian pulses in the (a) time and (b) frequency domain. Resultant waveform (c) and its spectrum (d).

TABLE II Gaussian-modulated Pulses.

Waveform	#1	#2	#3	#4
f_c, [MHz]	100	400	1000	400
FBW, [MHz]		$0.2 \times f_c$		f_c

TABLE III Gaussian-combination Waveforms.

Waveform	#1	#2
Frequency interval, [MHz]	30 ~ 400	80 ~ 1000
Number of Gaussian-modulated pulses	38	93
FBW of each pulse, [MHz]	10	

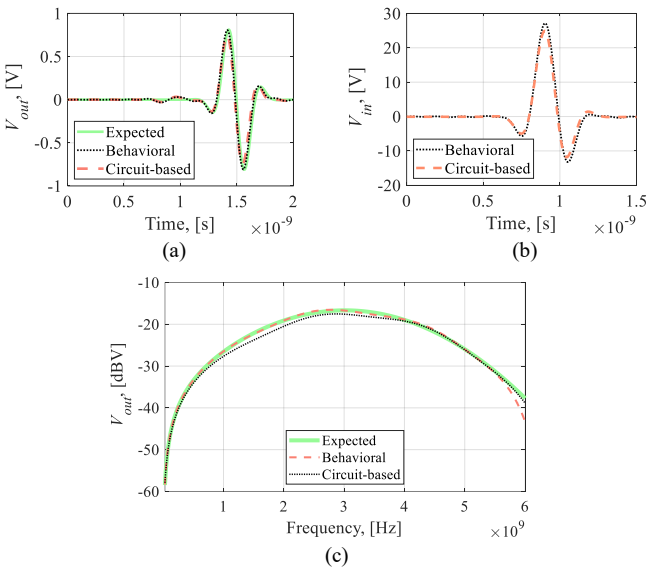

Fig. 9. Validation of the proposed equalization method: (a) Output waveforms (the green curve is the target waveform); (b) Predicted input waveforms, (c) Spectra of the output waveforms.

voltage $v_{out}(t)$ expected at the pins of the IC under test, the proposed procedure is aimed at deriving the input waveform $v_{in}(t)$ to be generated by the AWG, so to compensate for the frequency response of the overall measurement chain.

To this final goal, the frequency spectrum $V_{out}(f)$ of the output waveform $V_{out}(t)$ is firstly evaluated by Fast Fourier Transform (FFT), and then combined with the transfer function $H_s(f)$ of the measurement chain to obtain the spectrum of the input waveform $V_{in}(f)$ as:

$$V_{in}(f) = H_S^{-1}(f) \cdot V_{out}(f) \tag{10}$$

Eventually, the input waveform $v_{in}(t)$ is obtained by Inverse FFT (IFFT).

In (10), the transfer function $H_s(f)$ accounts for all the effects introduced by the measurement chain, including not only the transfer function introduced by the near-field probe as well as propagation effects along the trace under test, but also those effects due to cables, adapters/attenuators, and RF amplifiers used to connect the AWG output to the probe input in the actual setup. Towards this goal, the availability of accurate models of the injection probe plays a fundamental role. Indeed, both the behavioral and circuit-based models presented in the previous sections (with model parameters adapted as in Sec. IV) can be successfully employed to predict by circuit simulation the transfer function between the probe input and the IC pins. The obtained transfer function will be then combined with the transfer function associated with the measurement chain from the AWG output to the probe input, which will be obtained by VNA measurement, as it will be exemplified in the next Section.

As a preliminary validation, the proposed equalization method is exploited to identify the input waveform required to inject the green waveform in Fig. 9(a) at one termination of the test setup in Fig. 1 (with geometrical/electrical characteristics as in Sec. II-B). To this end, the default broadband pulse available in the HFSS transient solver is used for the sake of simplicity and to cover the whole frequency interval of interest

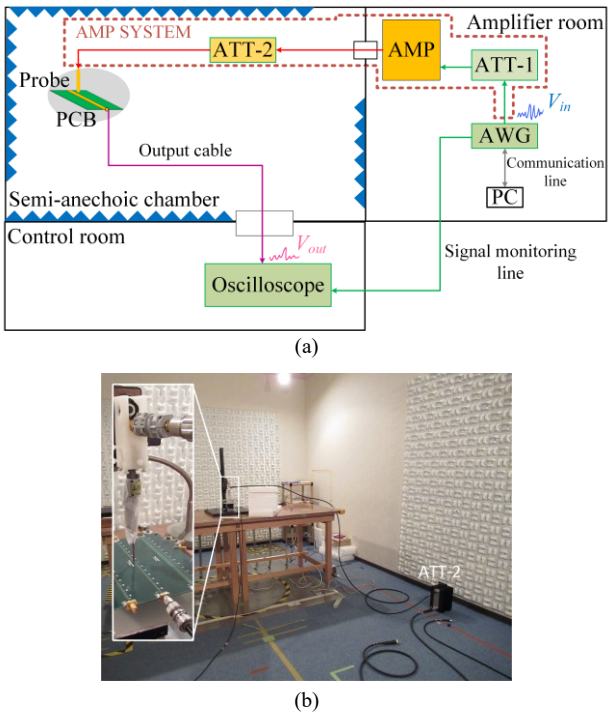

Fig. 10. Setup for time-domain immunity testing through near-filed probes: a) Principle drawing; and b) Picture of the test bench inside the semi-anechoic chamber.

with one simulation only. The proposed equalization procedure was used in combination with both the behavioral and the circuit-based models of the probe, yielding the input waveforms plotted in Fig. 9(b). These waveforms were then used as the inputs for HFSS simulation. The comparison of the obtained output waveforms versus the desired waveform in Fig. 9(a) shows an excellent agreement, which is also confirmed by the comparison of the corresponding spectra shown in Fig. 9(c), in the frequency interval up to 6 GHz.

VI. Experimental Assessment

A. Description of the test setup

A principle drawing of the measurement setup is shown in Fig. 10(a). Likewise for traditional immunity test procedures, the test bench was set up inside a semi-anechoic chamber. The AWG Keysight M8190A and the RF power amplifiers were installed into a nearby room, connected with the semi-anechoic chamber through coaxial cables. More specifically, two power amplifiers (AMP), i.e., a Prana DR220D with range 30 MHz~400 MHz and a MT700DC with range 80 MHz~1 GHz, equipped with suitable attenuators (ATT-1 & -2) were used to cover the frequency range from 30 MHz up to 1 GHz. A positioner was used to keep the near-field probe RG405 at midpoint of the trace under test. The trace is 134 mm long with nominal width w = 0.15 mm and thickness t = 35 µm. Also, it is covered by a 30 µm thick solder mask PSR-4000 MP, with dielectric permittivity ε_r = 4.7 at 1 MHz. The PCB substrate has thickness h = 80 µm, and it is made of FR4 R1551 with dielectric permittivity ε_r = 4.7 at 1 GHz, and loss tangent tanδ = 0.011 at 1 GHz. At the terminals, the trace is connected to a pair of SMA connectors. Finally, an oscilloscope Tektronix

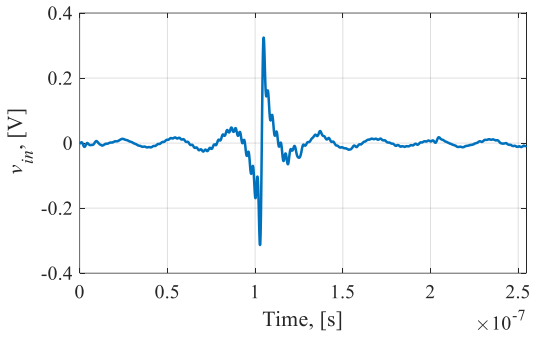

Fig. 11. Input waveform, v_{in}, required to inject the Gaussian-combination waveform in Fig. 12(e) at the terminations of the trace under test.

TDS6804B, connected to one trace terminal, is used to monitor the output waveform, v_{out}. To ensure measurement accuracy, the oscilloscope channel impedance was set to 50 Ω. However, it is worth mentioning that the models here proposed allow for simulation of the transfer function for whatever impedance seen looking into the IC pins and not for 50 Ω only. For systems characterized by the presence of different terminal impedances, new transfer functions can be derived by circuit simulation, and used to derive the input waveforms required to perform the test.

B. Measurement results

In order to identify the input waveforms required to induce at the terminations of the trace under test the waveforms in Tab. II and Tab. III, the transfer function associated with the measurement chain from the AWG output to the probe input was preliminary characterized by measurement. To this end, the S-parameters of (a) the AMP system (area denoted as "AMP SYSTEM" in Fig. 10(a)) and (b) the output cable to the oscilloscope were measured by a VNA Keysight E5071C. The obtained transfer functions were combined with the transfer function from the probe input to the trace output, which was predicted by exploiting the proposed circuit-based model (whose parameters were suitably adapted to the PCB under test by the correction factor introduced in Sec. IV), to obtain the overall transfer function $H_s(f)$ in (10). Then $V_{in}(f)$ is computed and transformed to the input waveform, v_{in}, to be generated by AWG and injected by the near-field probe during the test. As an explicative example, the input waveform required to obtain at the DUT pins the expected (output) waveform in Fig. 12(e) is shown in Fig. 11.

The comparison in Fig. 12 indicates that, for the output waveforms assigned in Tab. II and Tab. III, injection of the input waveforms evaluated by the proposed equalization procedure assures satisfactory agreement between the expected waveforms (green solid curves in the plots in Fig. 12), thus validating the proposed approach.

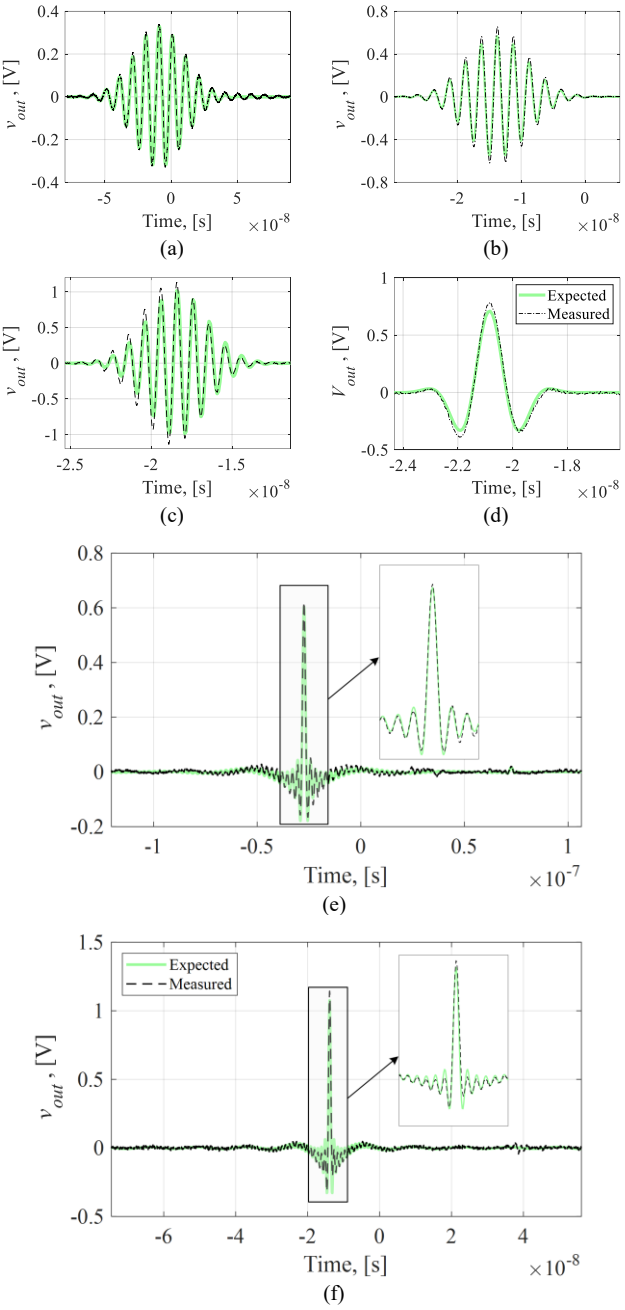

Fig. 12. Comparison between the expected waveforms and those actually measured when the input waveforms determined by the proposed equalization method are injected.: Waveform (a) No. 1, (b) No. 2, (c) No. 3 and (d) No. 4 in Table II; Waveform (e) No. 1 and (f) No. 2 in Table III.

VII. Conclusion

In this work, a test methodology has been introduced, aimed at investigating the possibility to design broadband immunity test procedures at PCB level using electric near-field probes as injection devices.

To this end, both behavioral and circuit-based modelling approaches were proposed to suitably represent the mechanism of probe-to-trace coupling. In this work, the analysis was focused on the electric near-field probes only, but the modelling procedures here proposed can also be extended to magnetic near-field probes, although their use for immunity testing is still under investigation. It has been proven that both the proposed models can be 1) implemented in circuit simulators; 2) used for both frequency- and time-domain simulations, and 3) easily adapted and used in combination with different PCBs and traces, by the introduction of empirical correction factors.

The proposed Gaussian-modulated pulses and suitable combinations of them can provide broadband frequency spectra, with customizable central frequency/bandwidth and flat

frequency response, respectively. Furthermore, it has been shown by measurement in a realistic test setup that the shape of the stress waveforms at the targeted pin can be precisely controlled by suitably equalizing the input waveform through the proposed circuit modelling and experimental characterization of the transfer function associated with the measurement chain. It follows the possibility to design and precisely control the shape of whatever stress waveforms, including those obtained from measurement, so to mimic practical interference waveforms encountered in real EM environment. These proposed models and techniques, which have proved to be compatible with traditional frequency-domain-based RF amplification systems, constitute the suitable and easy-to-implement methodology for test design of broadband time-domain immunity investigations.

REFERENCES

[1] Y. Gao and I. Wolf, "Miniature electric near-field probe for measuring 3D fields in planar microwave circuits," *IEEE Trans. Microw. Theory Tech.*, vol. 46, pp. 907–913, July 1998.

[2] Z. Yan, W. Liu, J. Wang, D. Su, X. Yan, and J. Fan, "Noncontact wideband current probes with high sensitivity and spatial resolution for noise location on PCB," *IEEE Trans. Instrum. Meas.*, vol. 67, no. 12, pp. 2881–2891, Dec. 2018.

[3] J. Shepherd, C. Marot, B. Vrignon and S. B. Dhia, "Near-field scan - State of the art and standardisation," in *Proc. Asia-Pacific Symp. Electromagn. Compat.*, Singapore, Singapore, May, 2012, pp. 1-4.

[4] A. Boyer, S. Benhia, and E. Sicard, "Characterization of electromagnetic susceptibility of integrated circuits using near-field scan," *Electron. Lett.*, vol. 43, no. 1, pp. 15–16, 2007.

[5] A. Boyer, B. Vrignon, J. Shepherd, and M. Cavarroc, "Evaluation of the near-field injection method at integrated circuit level," in *Proc. Electromagn. Compat. Europe*, Sep. 1–4, 2014, Goteborg, Sweden, pp. 85–90.

[6] *Integrated Circuits - Measurement of Electromagnetic Immunity - Part 9: surface scan method*, IEC Standard TS 62132-9*,* 2014.

[7] M. Girard, T., Dubois, G., Duchamp, and P., Hoffmann, "EMC susceptibility characterization of an operational amplifier-based circuit combining different technique". in *Proc. Electromagn. Compat. Europe*, Sep. 5–9, 2016, Wroclaw, Poland, pp. 300–305.

[8] T. Dubois, S. Jarrix, A. Penarier, P. Nouvel, D. Gasquet, L. Chusseau and B. Azais, "Near-Field Electromagnetic Characterization and Perturbation of Logic Circuits," *IEEE Trans. Instrum. Meas.*, vol. 57, no. 11, pp. 2398–2404, Feb. 2008.

[9] X. Wu, F. Grassi, G. Spadacini, S. A. Pignari, U. Paoletti and I. Hoda, "Investigation of Semi-Rigid Coaxial Test Probes as RF Injection Devices for Immunity Tests at PCB Level," in *IEEE Access*, vol. 8, pp. 147919-147929, 2020.

[10] X. Wu, F. Grassi, S. A. Pignari, U. Paoletti and I. Hoda, "Performance of Electric Near-Field Probes for Immunity Tests," in *Proc. XXXIII General Assembly Sci. Symp. Int. Union Radio Sci., (URSI GASS)*, Online, pp. 1-4, 2020

[11] C. F. M. Carobbi, A. Bonci, M. Stellini and M. Borsero, "Time-Domain Characterization of the Surge, EFT/Burst, and ESD Measurement Systems," in *IEEE Trans. Instrum. Meas.,* vol. 62, no. 6, pp. 1840-1846, June 2013

[12] D. Pommerenke, G. Muchaidze, J. Koo, Q. Cai, and J. Min, "Application and limits of IC and PCB scanning methods for immunity analysis," in *Proc. 18th Int. Zurich Symp. Electromagn. Compat.*, 2007, pp. 83–86.

[13] G. Muchaidze, J. Koo, Q. Cai, T. Li, L. Han, A. Martwick, K. Wang, J. Min, J. L. Drewniak, and D. Pommerenke, "Susceptibility scanning as a failure analysis tool for system-level electrostatic discharge (ESD) problems," *IEEE Trans. Electromagn. Compat.*, vol. 50, no. 2, pp. 268–276, May 2008.

[14] B. Ravelo, Y. Liu and A. K. Jastrzebski, "PCB Near-Field Transient Emission Time-Domain Model," in *IEEE Trans. Electromagn. Compat.*, vol. 57, no. 6, pp. 1320-1328, Dec. 2015,

[15] T. Liang, G. Spadacini, F. Grassi and S. A. Pignari, "Coupling of Wideband Radiated IEMI to Cables Above Ground," in *IEEE Trans. Electromagn. Compat.*, vol. 62, no. 2, pp. 589-597, Apr. 2020

[16] X. Tong, D. W. P. Thomas, A. Nothofer, P. Sewell, and C. Christopoulos, "Modeling Electromagnetic Emissions From Printed Circuit Boards in Closed Environments Using Equivalent Dipoles" *IEEE Trans. Electromagn. Compat.*, vol. 52, no. 3, pp 462-470, May 2010

[17] D. Baudry, C. Arcambal, A. Louis, B. Mazari, and P. Eudeline, "Applications of the near-field techniques in EMC investigations," *IEEE Trans. Electromagn. Compat.*, vol. 49, no. 4, pp. 805–815, Nov. 2007.

[18] A. Durier, S. Ben Dhia and T. Dubois, "Comparison of voltages induced in an electronic equipment during far field and near field normative radiated immunity tests," in *Proc. IEEE Int. Symp. Electromagn. Compat.- EMC Europe,* Barcelona, Spain, 2019, pp. 938-943

[19] F. Hiroki, T. Suga, and M. Suhara. "Improved position-signal-difference electric near-field measurements based on fringe capacitance model." *IEICE Electronics Express* vol. 11, no. 11 20140272-20140272, 2014.

[20] W. Fang, H. Qiu, C. Luo, L. Wang, W. Shao, E. Shao, S. Li and Y. En, "Noncontact RF Voltage Sensing of a Printed Trace via a Capacitive-Coupled Probe," in *IEEE Sensors Journal*, vol. 18, no. 21, pp. 8873-8882, Nov. 2018.

[21] S. Atrous, D. Baudry, E. Gaboriaud, A. Louis, B. Mazari and D. Blavette, "Near-field investigation of the radiated susceptibility of printed circuit boards," in *Proc. IEEE Int. Symp. Electromagn. Compat.- EMC Europe*, Hamburg, Germany, Sep. 2008, pp. 1–6.

[22] A. K. Agrawal, H. J. Price and S. H. Gurbaxani, "Transient Response of Multiconductor Transmission Lines Excited by a Nonuniform Electromagnetic Field," in *IEEE Trans. Electromagn. Compat.*, vol. EMC-22, no. 2, pp. 119-129, May 1980

[23] F. Grassi, F. Marliani and S. A. Pignari, "Circuit modeling of injection probes for bulk current injection", *IEEE Trans. Electromagn. Compat.*, vol. 49, no. 3, pp. 563-576, Aug. 2007.